Impact of Sulfur vs Oxygen on the Low-Lying Excited States of *trans-p*-Coumaric Acid and *trans-p*-Coumaric Thio Acid

Evgeniy V. Gromov,*,†,§ Irene Burghardt,‡ Horst Köppel,† and Lorenz S. Cederbaum†

Theoretische Chemie, Physikalisch-Chemisches Institut, Universität Heidelberg, Im Neuenheimer Feld 229, D-69120 Heidelberg, Germany, Laboratory of Quantum Chemistry, Computer Center, Irkutsk State University, K. Marks 1, 664003 Irkutsk, Russian Federation, and Département de Chimie, Ecole Normale Supérieure, 24 rue Lhomond, F-75231 Paris Cedex 05, France

Received: November 15, 2004; In Final Form: March 24, 2005

The low-lying excited singlet states of *trans-p*-coumaric acid (CA) and *trans-p*-coumaric thio acid (CTA) are investigated in view of characterizing the chromophore of the photoactive yellow protein (PYP), with particular regard to the impact of sulfur on the chromophore's electronic structure. The comparative ab initio study, performed with the highly accurate EOM-CCSD method, shows that the electronic state ordering upon vertical excitation and following in-plane geometry relaxation indeed depends in a very sensitive fashion on the presence of either sulfur or oxygen. The study identifies three relevant excited singlet states, two of which are of $\pi-\pi^*$ type while the third state is of $n-\pi^*$ character. The study highlights the role of the latter $n-\pi^*$ state which is shown to be the lowest-lying excited state of CTA at all in-plane geometries under consideration, whereas this is not the case for CA.

I. Introduction

The electronic structure of the excited states of coumaric acid (CA) and its sulfur containing analogue, coumaric thio acid (CTA; Figure 1), has recently attracted much interest, in view of investigating the photochemical processes in the photoactive yellow protein (PYP). PYP is a photoreceptor protein occurring in halophilic bacteria, which mediates the repulsive motional response of these bacteria to blue light (negative phototaxis).[1−3] Its chromophore is the *trans-p*-hydroxythiocinnamate anion (i.e., the phenolate anion of coumaric thio acid) which is covalently bound to a cysteine residue of the protein via a thioester linkage.[3−5] The earliest, subpicosecond events in the photocycle of PYP are thought to involve the isomerization of the chromophore's double bond,[3−7] via a S_1-S_0 conical intersection,[8−10] thus initiating the further steps in the photocycle. At a later stage of the cycle, the chromophore is protonated. Besides experimental studies of the native protein, the PYP chromophore has been investigated in the denatured form of the protein[11,12] and in solution phase.[12−16] Although no experimental study to date seems to have addressed the isolated, neutral coumaric thio acid and its ester derivatives, a gas phase study of neutral coumaric acid has been carried out by Levy and co-workers.[17] These experiments provide strong indications that several excited electronic states are involved, for both the neutral and anionic species. Furthermore, the experiments point to the extreme sensitivity of the spectroscopic properties and photochemical processes to the details of the chromophore's local environment[11,12] as well as the chemical nature of the substituents bound to the coumaric acid group.[12,18]

On the theory side, recent electronic structure studies have addressed different aspects in connection with the experimental observations. Martínez and co-workers carried out calculations for the low-lying excited states of the neutral coumaric acid chromophore[8] and identified several conical intersections. Molina and Merchán[19] addressed selected geometries of the methyl thioester of the coumaric acid chromophore, corresponding to different intermediates of the photocycle. In a time-dependent density functional theory (TDDFT) study for a model of the PYP active site, Thompson et al.[20] mapped out the isomerization and proton transfer steps of the photocycle, on a time scale up to nanoseconds. Groenhof et al.[21] used combined

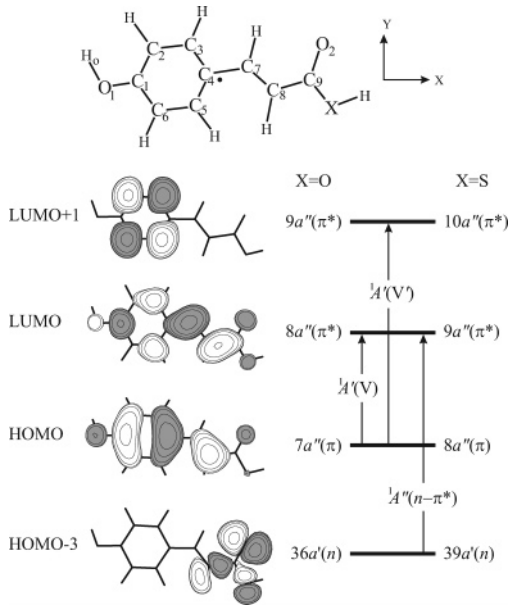

Figure 1. Upper part: Ground-state equilibrium geometry of coumaric acid (X=O) and coumaric thio acid (X=S) [the point marked in the figure denotes the coordinate origin]; lower part: relevant valence orbitals and low-lying electronic transitions of coumaric acid and coumaric thio acid.

* To whom correspondence should be addressed.
† Universität Heidelberg.
§ Irkutsk State University.
‡ Ecole Normale Supérieure.

10.1021/jp0447791 CCC: $30.25
Published on Web 05/03/2005

TDDFT and molecular dynamics simulations to study the isomerization transition state and more recently undertook excited-state quantum mechanics/molecular mechanics (QM/MM) calculations[10] characterizing the S_1-S_0 conical intersection in the protein environment. Finally, Yamada et al.[22] used the QM/MM (ONIOM) method to characterize the "driving force" for the isomerization at a microscopic level.

The above experimental and theoretical studies have identified the following factors which have a key impact upon the properties and spectroscopy of the chromophore: (i) the effects of the local environment, in the protein or in solution phase, (ii) the anionic or neutral nature of the chromophore, and (iii) the role of sulfur as compared with oxygen in the coumaric ester bond (which, in the protein, links the chromophore to the protein pocket). The present work focuses on the third aspect, which has not been investigated in detail as yet. In this first study, we consider the neutral *trans-p*-CA and its sulfur substituted analogue, *trans-p*-CTA, and compare the low-lying excited singlet states of both species. It is shown that the electronic structure properties of the excited states indeed depend in a very sensitive fashion on the presence of either oxygen or sulfur in the chromophore. Besides the role of two close-lying $\pi-\pi^*$ excited states, the present study highlights the presence of an $n-\pi^*$ state, which is the lowest-lying excited state in CTA at all (in-plane) geometries considered. In contrast, the situation is significantly different in the case of CA.

Given that the active form of the chromophore at the earliest, subpicosecond and picosecond stages of the photocycle, is the anionic rather than neutral species (the chromophore is protonated much later, on a microsecond time scale[2]), our results for CTA cannot be directly related to experimental observations of the excited-state processes occurring during the initial steps of the photocycle. Indeed, preliminary calculations which we undertook for the anionic chromophore, as briefly summarized in the Concluding Remarks, provide evidence for pronounced differences between the electronic structure of the neutral vs anionic species, in accordance with earlier observations in ref 19. We do not propose a detailed discussion of the anionic species in the present work, since the isolated CA^- and CTA^- chromophores exhibit autoionizing excited states (i.e., metastable states lying in the ionization continuum)[23,24] which require an appropriate electronic structure treatment. A detailed characterization of these species will therefore be reserved for future studies. As an additional remark, the protein environment is expected to significantly stabilize the anionic chromophore by the presence of counterions (thus increasing the ionization potential to create true bound states).[23] Hence, the actual electronic structure of the chromophore is expected to be significantly influenced by the environment and can be thought of as intermediate between the anionic and neutral species.

In the present work, the excited states of CA and CTA have been characterized by the equation-of-motion coupled-cluster singles and doubles (EOM-CCSD) approach.[25-27] The EOM-CCSD method properly takes electron correlation effects into account and possesses high accuracy. As a further advantage for the present study, analytical energy gradients are available,[28] making feasible a full geometry optimization for the excited states. Finally, one should mention the size-consistency property of the coupled cluster approach, in addition to the possibility to use it in large-scale rooting calculations.

Finally, it is worthwhile to note that *p*-coumaric acid is of high importance itself due to the known anti-cancer activity of this substance.[29] The present study is thus of interest in this regard as well.

II. Computational Details

The ground-state geometry of the trans forms of CA and CTA, respectively, was optimized using the conventional CCSD method,[30] to be consistent with the EOM-CCSD level of description for the excited states. The 6-31G* basis set was employed throughout.[31] Among several isomers of the chromophores (see discussion below), the thermodynamically most favorable one was identified; all excited-state calculations were carried out for this most stable isomer. The minimum character of the ground-state structure was verified.[32]

The full (in-plane) geometry optimization for the excited states was performed by the EOM-CCSD method via the analytical energy gradient technique.[28] At each stationary point obtained, including the ground-state equilibrium geometry, the properties of the relevant excited states—excitation energies, oscillator strengths, dipole moments and charge distributions—were computed with the same ab initio approach. The type of the excited state stationary points (minima or transition states) will be addressed in forthcoming work, given that the usual vibrational analysis, i.e., calculation of vibrational frequencies at the points in question, represents a challenging computational task at the EOM-CCSD level for systems of this size (54 vibrational degrees of freedom). Specifically, no analytical second derivative computational technique is currently available for EOM-CCSD energies.

In all excited-state calculations, the 6-31G* basis set[31] was used, in conjunction with the five-component representation of the d functions. The total number of molecular orbitals was 184 and 188 for CA and CTA, respectively. The core orbitals were kept frozen in all ground and excited-state coupled-cluster calculations.

The ground and excited-state geometry optimizations were performed using the ACES II ab initio program package.[33] For separate calculations of the vertical excitation energies, we also used the MOLPRO program set[34] where a very efficient version of the EOM-CCSD method is available.

III. Results

A. $\tilde{X}^1A'$ Ground State of CA and CTA. In their respective electronic ground states, CA and CTA have a planar equilibrium configuration of C_s symmetry, depicted in Figure 1; this configuration accommodates the presence of the phenolic ring, the $C_7=C_8$ double bond, and the $C_9=O_2$ carboxylic bond. Four relevant planar isomers (all of trans type; the rotation of the X−H group is not considered) exist which are distinguished by (i) the position of the two double bonds with respect to the C_8-C_9 single bond (s-cis for the double bonds lying on the same side of the single bond, and s-trans for the double bonds on opposite sides) and (ii) the position of the phenolic hydrogen H_o with respect to the carbonyl oxygen of the para-substituent (here denoted as syn vs anti isomers). According to our CCSD ground state optimization calculations (Table 1), the thermodynamically most favorable form for both CA and CTA is the s-cis-syn isomer. The other isomers are slightly higher in energy, with a difference of about 1.0 kcal/mol between the s-cis and s-trans isomers, and, as expected, a much smaller difference of about 0.1 kcal/mol between the syn and anti isomers. (For comparison, the difference between trans and cis isomers with respect to the $C_7=C_8$ double bond is about 4 kcal/mol.) Table 1 also summarizes corresponding results obtained by the DFT-(B3LYP)/6-31G** and MP2/6-31G* methods, all of which corroborate the CCSD predictions.

Selected ground state geometrical characteristics of the (energetically most favorable) s-cis-syn isomer of CA and CTA

TABLE 1: Total Ground State Energies of Four Relevant Isomers of CA and CTA as Predicted by Optimization with the CCSD, DFT, and MP2 Approaches

	CCSD/6-31G*		DFT/6-31G**		MP2/6-31G*
isomer	CA	CTA	CA	CTA	CA
s-cis-syn	−571.757238	−894.344210	−573.462684	−896.414835	−571.725801[a]
s-cis-anti	−571.757042	−894.344006	−573.462530	−896.414689	−571.725616
s-trans-syn	−571.755685	−894.341712	−573.461151	−896.411900	−571.724255
s-trans-anti	−571.755779	−894.341817			

[a] Corresponds to a transition state, associated with an imaginary frequency of *a″* symmetry as obtained by vibrational analysis (see text for details).

TABLE 2: Ground State Geometrical Parameters for s-cis-syn-CA and -CTA Obtained with the CCSD, DFT, and MP2 Approaches

	CCSD/6-31G*		DFT/6-31G**		MP2/6-31G*
parameter	CA	CTA	CA	CTA	CA
O_1-C_1	1.371	1.370	1.361	1.360	1.371
C_1-C_2	1.396	1.396	1.399	1.399	1.397
C_2-C_3	1.397	1.396	1.390	1.390	1.393
C_3-C_4	1.402	1.402	1.407	1.407	1.404
C_4-C_5	1.410	1.410	1.411	1.412	1.408
C_5-C_6	1.388	1.388	1.386	1.385	1.388
C_6-C_1	1.403	1.403	1.403	1.404	1.400
C_4-C_7	1.470	1.469	1.458	1.455	1.460
C_7-C_8	1.346	1.347	1.347	1.350	1.348
C_8-C_9	1.479	1.483	1.471	1.471	1.473
C_9-O_2	1.217	1.217	1.218	1.213	1.222
C_9-X	1.359	1.802	1.361	1.832	1.364

obtained with CCSD optimization are presented in Table 2. For comparison, the table also gives corresponding results obtained by the DFT and MP2 methods. As can be seen, all sets of theoretical data are in very good agreement, with deviations with respect to the bond lengths reported not exceeding 0.01 Å. The same holds for the remaining bond lengths and valence angles (not shown in the table); angles vary by no more than 1°.

Despite the overall good agreement, a noticeable difference occurs between the CCSD vs DFT/MP2 results regarding the C_4-C_7 bond length, which is longer by 0.01 Å according to our CCSD calculations. The shorter bond length predicted by the MP2 method most likely correlates with the instability of the planar s-cis-syn isomers of CA and CTA with respect to small rotations about the C_4-C_7 bond found at this level of calculation (see Table 1). This instability is neither predicted by CCSD nor, interestingly, by DFT (even though DFT also underestimates the bond length); both CCSD and DFT thus predict the planar configuration to be a true minimum. The MP2 result should be considered an artifact (especially given that planar and nonplanar stationary points differ merely by thousandths of kcal/mol) and is presumably related to the significant role of electron correlation effects in the ground states of CA and CTA. More specifically, the CCSD wave function features a relatively high weight of doubly excited configurations (of about 30%). Such situations are apparently not well described at the MP2 level.

B. Orbital Pattern of CA and CTA. The ground state (Hartree−Fock) electronic configurations of both systems are similar and reveal the same types of highest occupied (HO) and lowest unoccupied (LU) molecular orbitals (MO). The most important orbitals are shown in Figure 1, from which one can infer that the HOMO and LUMO are of π and π^* type, respectively. Given that the HOMO → LUMO transition is accompanied by a change in bonding → antibonding patterns with respect to the $C_7=C_8$ double bond, this transition is expected to play a key role in the trans−cis isomerization of the chromophore. A second low-lying π^* orbital exists, denoted (LUMO+1), with a predominant location within the aromatic ring. Further, the figure shows an orbital denoted (HOMO-3), which is an *n*-type (nonbonding) orbital related to the lone pair of the heteroatom. As will become apparent below, the orbitals shown prove to be the most relevant for the low-energy excitations in CA and CTA.

In the following, two low-lying excited singlet states of A′ symmetry are denoted as $^1A'(V)$ and $^1A'(V')$ (V stands for "valence"). Although these states can mix, we distinguish them (where possible) on the basis of their principal configurations or/and differences in their oscillator strengths (see below). The $^1A'$ states result from $\pi-\pi^*$ excitations, involving mostly the HOMO → LUMO transition in the case of $^1A'(V)$ and the HOMO → (LUMO+1) transition in the case of $^1A'(V')$ (see Figure 1). A further low-lying excited singlet state, of A″ symmetry, has a principal configuration stemming from the *n* → LUMO electronic transition and is denoted $^1A''(n-\pi^*)$.

Although the pattern of (Hartree−Fock) orbital energies and shapes is very similar for CA and CTA, the energetic ordering of states will turn out to be significantly different. Anticipating the discussion in section IV.A, this is primarily due to a shift in energy of the (HOMO-3) *n*-type orbital; the presence of sulfur vs oxygen strongly impacts upon the relevant orbital energy.

C. Lowest Excited States of CA and CTA. In the following, we focus on the lowest excited singlet states of CA and CTA. We will consider transition energies and oscillator strengths at selected geometries of the chromophores. In this first study, all calculations were restricted to the in-plane geometry of the molecules; forthcoming studies will address torsional displacements that are key for the trans−cis isomerization. The geometries in question are the equilibrium configuration of the ground state ($\tilde{X}^1A'$) and the constrained, in-plane equilibrium configurations of the excited states. For the vertical transitions, i.e., transitions at the ground-state equilibrium configuration, results can be compared with previous studies by Martínez and co-workers[8] for CA and, on a more qualitative level, a study by Molina and Merchán[19] for the methyl thioester of CTA.

As a remark on nomenclature, the adiabatic potential energy surfaces (PESs) of the singlet states are denoted as S_0, S_1, S_2, etc. The S_i surfaces thus correspond to the energies obtained as the $(i+1)$st root of the Hamiltonian at all nuclear conformations. Note further that we make use of spectroscopic terminology, by which distinct stationary points of a PES are denoted as "states".

1. Vertical Excitations in CA. According to the EOM-CCSD calculations reported in Table 3, the first three lowest excited singlet states of CA correspond to $^1A'(V')$, $^1A'(V)$, and $^1A''(n-\pi^*)$ in order of increasing transition energy (see first row of Table 3, $\tilde{X}^1A'$ geometry). These states cover a rather narrow energy window of about 0.5 eV, between 4.8 and 5.3 eV. The EOM-CCSD transition energies of Table 3 are in fair agreement with corresponding EOM-CCSD results by Martínez and co-

TABLE 3: Energies[a] and Oscillator Strengths for the Lowest Excited Singlet States of CA for Different Geometries[b] of the Molecule

		transition energies			oscillator strengths		
geometry	method	$^1A'(V')$	$^1A'(V)$	$^1A''(n-\pi^*)$	$^1A'(V')$	$^1A'(V)$	$^1A''(n-\pi^*)$
$\tilde{X}^1A'$	EOM-CCSD	4.84	5.13	5.30	0.061	0.739	< 0.001
	EOM-CCSD[c]	4.92	5.14	5.55			
	CIS/6-31G*	5.86	5.26	6.47	0.015	0.806	< 0.001
$^1A'(V')$	EOM-CCSD	4.67	5.03	5.35	0.138	0.664	< 0.001
$^1A'(V)$	EOM-CCSD	4.81	4.84	5.22	0.389	0.447	< 0.001
$^1A''(n-\pi^*)$	EOM-CCSD	5.67	5.32	4.53	0.024	0.794	< 0.001

[a] For all our EOM-CCSD and CIS results, the corresponding CCSD and HF energy calculated at the $\tilde{X}^1A'$ geometry is taken as origin. [b] See text for details. [c] Reference 8.

TABLE 4: Ground and Excited State Dipole Moments (a.u.) at the Equilibrium Geometry of the Ground State

electronic state	$\langle x \rangle$	$\langle y \rangle$	$\langle z \rangle$
coumaric acid			
$\tilde{X}^1A'$	−0.763	0.134	0.0
$^1A'(V')$	−1.145	0.224	0.0
$^1A'(V)$	−3.278	0.020	0.0
$^1A''(n-\pi^*)$	1.111	0.638	0.0
coumaric thio acid			
$\tilde{X}^1A'$	−1.086	0.152	0.0
$^1A'(V')$	−2.375	0.195	0.0
$^1A'(V)$	−3.117	−0.199	0.0
$^1A''(n-\pi^*)$	0.469	0.428	0.0

workers;[8] the maximal deviation occurs for the $^1A''(n-\pi^*)$ state (0.25 eV). We attribute this deviation to the differences in the molecular geometry, in particular for the position of the phenolic group (relating to the syn vs anti isomers discussed above).

To estimate the importance of electron correlation for the excited states under consideration (in particular regarding doubly excited configurations), we performed calculations for vertical excitations using the configuration interaction singles (CIS) method.[35] On comparing EOM-CCSD and CIS transition energies (Table 3), substantial discrepancies are apparent, affecting the electronic states in a very different fashion. Although the deviation for the $^1A'(V)$ state is small (0.13 eV), the differences for the $^1A'(V')$ and $^1A''(n-\pi^*)$ states are of about 1 eV, such that the $^1A'(V)$ state is predicted to be the lowest excited-state according to the CIS calculation. The same qualitative result was obtained in a TDDFT study by Sergi et al.;[36] the predicted excitation energy for the $^1A'(V)$ state (3.76 eV) was however far too low. The above clearly signifies that methods such as CIS and TDDFT which do not properly account for electron correlation effects are not appropriate for the study of the systems under consideration.

EOM-CCSD predictions of the oscillator strengths (Table 3) show that the most intense low-lying vertical transition is to the $^1A'(V)$ excited state. This transition is about 1 order of magnitude stronger than that to the $^1A'(V')$ excited state. The oscillator strength of excitation to the $^1A''(n-\pi^*)$ state is extremely low. This is not unexpected since the n and π^* orbitals in question have little overlap.

Table 4 summarizes the dipole moments calculated at the $\tilde{X}^1A'$ geometry. Pronounced changes in dipole moments with respect to the ground state are observed for the $^1A'(V)$ and $^1A''(n-\pi^*)$ states. Specifically, the $^1A'(V)$ state features a substantial increase in the absolute value of the dipole moment, whereas in the $^1A''(n-\pi^*)$ state, the dipole moment direction is reversed. This suggests significant charge migration effects between the phenolic ring and the alkyl fragment. To further clarify this point, we calculated atomic charges in the $\tilde{X}^1A'$ ground state and the excited states under consideration, see Table 5. As can be inferred from the table, a substantial charge redistribution indeed occurs in the $^1A'(V)$ and $^1A''(n-\pi^*)$ states. For the $^1A'(V)$ state, a charge migration of about 0.21 "electrons" is observed from the phenolic ring to the alkyl fragment, in accordance with the dipole moment values. By contrast, a reversed charge transfer of about 0.09 "electrons" takes place in the case of the $^1A''(n \rightarrow \pi^*)$ state. The electronic distribution in the $^1A'(V')$ state is similar to the ground state.

TABLE 5: CCSD Prediction of the Atomic Charge Distributions[a] for the Ground and Three Lowest Excited Singlet States of CA Calculated at the $\tilde{X}^1A'$ Geometry

atom	$\tilde{X}^1A'$		$^1A'(V')$		$^1A'(V)$		$^1A''(n-\pi^*)$	
O_1	−0.26	+0.07[b]	−0.23	+0.08[b]	−0.20	+0.28	−0.28	−0.02[b]
C_1	+0.38		+0.37		+0.39		+0.37	
C_2	−0.08		−0.09		−0.03		−0.09	
C_3	−0.01		+0.01		0.00		−0.03	
C_4	+0.04		+0.07		+0.05		+0.06	
C_5	+0.01		−0.04		+0.07		−0.03	
C_6	−0.01		−0.01		0.00		−0.02	
C_7	+0.07	−0.07[c]	+0.05	−0.08[c]	+0.04	−0.28[c]	−0.05	+0.02[c]
C_8	−0.08		−0.07		−0.15		−0.03	
C_9	+0.64		+0.64		+0.60		+0.53	
O_2	−0.48		−0.48		−0.52		−0.25	
X=O	−0.22		−0.22		−0.25		−0.18	

[a] Charges on hydrogens are included on the neighboring atoms. [b] Sum of charges for the phenolic group of atoms. [c] Sum of charges for the alkyl group of atoms.

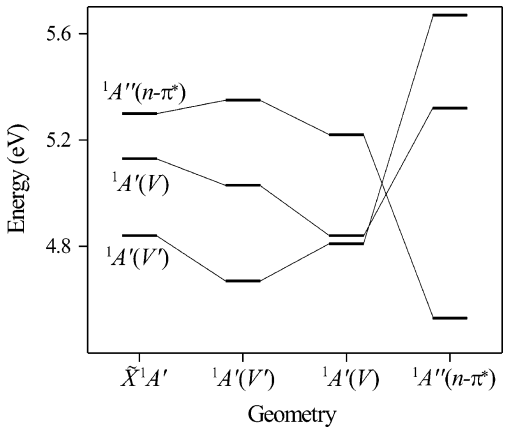

Figure 2. Schematic diagram showing the low-lying singlet excited states of coumaric acid (CA) at the optimized geometry of the ground $\tilde{X}^1A'$ state and at the respective in-plane optimized geometries of the $^1A'(V')$, $^1A'(V)$, and $^1A''(n-\pi^*)$ excited states.

2. Geometry Relaxation in Excited CA. Figure 2 depicts the results of in-plane geometry optimization for the $^1A'(V')$, $^1A'(V)$, and $^1A''(n-\pi^*)$ excited states of CA, on the grounds of the EOM-CCSD data reported in Table 3. In the figure, the stationary points corresponding to the $^1A'(V')$, $^1A'(V)$, and $^1A''(n-\pi^*)$ (constrained, in-plane) equilibrium geometries are fixed along the horizontal axis, and a cut through the S_1, S_2,

TABLE 6: Selected Bond Lengths at the Equilibrium Geometry of the Ground State and In-Plane Equilibrium Geometries of the Excited States

	coumaric acid				coumaric thio acid			
parameter	$\tilde{X}^1A'$	$^1A'(V')$	$^1A'(V)$	$^1A''(n-\pi^*)$	$\tilde{X}^1A'$	$^1A'(V')$	$^1A'(V)$	$^1A''(n-\pi^*)$
O_1-C_1	1.371	1.360	1.356	1.376	1.370	1.361	1.346	1.375
C_1-C_2	1.396	1.425	1.418	1.396	1.396	1.418	1.427	1.396
C_2-C_3	1.397	1.404	1.416	1.395	1.396	1.428	1.369	1.396
C_3-C_4	1.402	1.442	1.439	1.407	1.402	1.437	1.445	1.406
C_4-C_5	1.410	1.435	1.452	1.413	1.410	1.444	1.447	1.413
C_5-C_6	1.388	1.433	1.386	1.390	1.388	1.404	1.384	1.389
C_6-C_1	1.403	1.414	1.421	1.400	1.403	1.418	1.410	1.401
C_4-C_7	1.470	1.434	1.421	1.457	1.469	1.429	1.406	1.459
C_7-C_8	1.346	1.367	1.388	1.388	1.347	1.374	1.420	1.381
C_8-C_9	1.479	1.469	1.449	1.380	1.483	1.463	1.428	1.399
C_9-O_2	1.217	1.222	1.231	1.344	1.217	1.225	1.243	1.323
C_9-X	1.359	1.362	1.371	1.369	1.802	1.811	1.826	1.789

TABLE 7: Energies[a] and Oscillator Strengths for the Lowest Excited Singlet States of CTA for Different Geometries[b] of the Molecule

		transition energies			oscillator strengths		
geometry	method	$^1A'(V')$	$^1A'(V)$	$^1A''(n-\pi^*)$	$^1A'(V')$	$^1A'(V)$	$^1A''(n-\pi^*)$
$\tilde{X}^1A'$	EOM-CCSD	4.79	4.93	4.31	0.348	0.556	< 0.001
	CIS/6-31G*	5.85	5.11	5.21	0.012	0.956	< 0.001
$^1A'(V')$	EOM-CCSD	4.75	4.69	4.34	0.234	0.689	< 0.001
$^1A'(V)$	EOM-CCSD	5.00	4.50	4.27	0.039	0.914	< 0.001
$^1A''(n-\pi^*)$	EOM-CCSD	5.37	4.98	3.83	0.019	0.880	< 0.001

[a] For all our EOM-CCSD and CIS results, the corresponding ground CCSD and HF energy calculated at the $\tilde{X}^1A'$ geometry is taken as origin. [b] See text for details.

and S_3 potential energy surfaces is shown at each point. As a reference for the results at excited-state geometries, we indicate the vertical excitation results (cut at the $\tilde{X}^1A'$ geometry) discussed in the preceding section.

The most pronounced effect of geometry relaxation clearly occurs at the $^1A''(n-\pi^*)$ equilibrium geometry. Here, the energy of the $^1A''(n-\pi^*)$ state is lowered by as much as 0.75 eV, and the state becomes the lowest excited state (S_1), in fact, energetically lower than the S_1 states at the other geometries under consideration. In addition, the respective ordering of the $^1A'(V')$ and $^1A'(V)$ states is exchanged at the $^1A''(n-\pi^*)$ geometry as compared to the $\tilde{X}^1A'$ geometry. This was concluded from the oscillator strength value for the first $^1A'$ excited state at the $^1A''(n-\pi^*)$ geometry, which is much higher than the corresponding value for the second $^1A'$ state, suggesting that the former should be assigned to $^1A'(V)$.

The $^1A'(V')$ and $^1A'(V)$ states are stabilized by 0.17 and 0.29 eV, respectively, as a result of geometry relaxation. Their energetic ordering relative to the $^1A''(n-\pi^*)$ state remains the same as for vertical transitions. However, one can see that at the $^1A'(V)$ stationary point, the $^1A'(V')$ and $^1A'(V)$ excited states closely approach each other, suggesting an avoided crossing situation. On the other hand, the $^1A'$ states were shown to interchange at the $^1A''(n-\pi^*)$ geometry (see above). Therefore, their PES intersect and one can very likely expect an intersection close to the $^1A'(V)$ geometry (as a general consequence of the Truhlar-Mead principle;[37] see also discussion in Ref. 38). Our prediction of a $^1A'(V')-^1A'(V)$ conical intersection is also in line with findings by Martínez and co-workers,[8] who provided evidence for a conical intersection of the S_1 and S_2 states at the planar geometry of molecule, involving only bond alterations.

In the following, we discuss the geometry changes accompanying the excited-state relaxations. Table 6 reports various bond lengths for the relaxed structures and includes corresponding results for CTA, to be discussed below. For the $^1A''(n-\pi^*)$ state, a marked elongation of the carbonyl $C_9=O_2$ double bond is observed, halfway approaching a single bond length, along with a strong contraction of the neighboring C_8-C_9 bond. Indeed, the C_7-C_8 and C_8-C_9 bond lengths become nearly identical. The mechanism underlying these changes is discussed in section IV. B.

The geometrical changes for the other excited states are different. The structure of the $^1A'(V')$ state exhibits a rather moderate geometry modification which essentially affects the aromatic fragment of the molecule, consistent with the antibonding character of the $9a''(\pi^*)$ MO involved in the $^1A'(V')$ excitation (see Figure 1). A rather pronounced alteration of the alkyl part occurs for the $^1A'(V)$ state. In the process, the $C_7=C_8$ double bond substantially extends, which can be interpreted as a result of populating the $8a''(\pi^*)$ MO whose character is antibonding for this bond. Clearly, this is a reflection of the fact that the $^1A'(V)$ state is involved in the trans−cis isomerization process (see below).

3. Vertical Excitations in CTA. At the equilibrium geometry of the $\tilde{X}^1A'$ ground state, our EOM-CCSD calculations reveal the following ordering of the three lowest excited singlet states of CTA: $^1A''(n-\pi^*)$, $^1A'(V')$, and $^1A'(V)$, in order of increasing energy (Table 7). The two $^1A'$ states mix substantially here, and their assignment should therefore be understood in an approximate fashion, based on differences in the oscillator strengths for the corresponding transitions. The state ordering for CTA is evidently different from CA at its ground-state equilibrium geometry. A dramatic lowering, of ∼1 eV, has occurred for the transition energy of the $^1A''(n-\pi^*)$ excited state. Moreover, one can see a moderate energy lowering for both the $^1A'(V')$ and $^1A'(V)$ states.

As observed before for the case of CA, transition energies at the CIS level of calculations deviate strongly from the EOM-CCSD results, by up to 1 eV. A comparison with results from the literature is possible only at a qualitative level, referring to a study of the methyl thioester of the coumaric acid chromophore carried out by Molina and Merchán.[19] Although these authors focused on the anionic species, they give selected results on the cis form of the neutral species (see structure IV in Ref.

TABLE 8: CCSD Prediction of the Atomic Charge Distributions[a] for the Ground and Three Lowest Excited Singlet States of CTA Calculated at the $\tilde{X}^1A'$ Geometry

atom	$\tilde{X}^1A'$		$^1A'(V')$		$^1A'(V)$		$^1A''(n-\pi^*)$	
O_1	−0.26	+0.08[b]	−0.22	+0.19[b]	−0.21	+0.24[b]	−0.27	0.0[b]
C_1	+0.38		+0.38		+0.38		+0.37	
C_2	−0.08		−0.09		−0.02		−0.08	
C_3	0.01		+0.06		−0.03		−0.03	
C_4	+0.04		+0.07		+0.05		+0.06	
C_5	0.00		−0.04		+0.08		−0.03	
C_6	−0.01		+0.02		−0.01		−0.02	
C_7	+0.08	−0.08[c]	+0.05	−0.18[c]	+0.06	−0.24[c]	−0.02	0.0[c]
C_8	−0.08		−0.09		−0.11		−0.02	
C_9	+0.26		+0.25		+0.24		+0.09	
O_2	−0.43		−0.46		−0.48		−0.26	
X=S	+0.09		+0.07		+0.05		+0.21	

[a] Charges on hydrogens are included on the neighboring atoms. [b] Sum of charges for the phenolic group of atoms. [c] Sum of charges for the alkyl group of atoms.

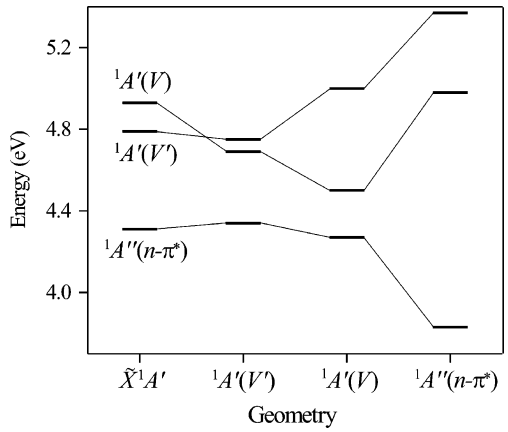

Figure 3. Schematic diagram showing the low-lying singlet excited states of coumaric thio acid (CTA) at the optimized geometry of the ground $\tilde{X}^1A'$ state and at the respective in-plane optimized geometries of the $^1A'(V')$, $^1A'(V)$, and $^1A''(n-\pi^*)$ excited states.

19), predicting that the $n-\pi^*$ transition is lowest in energy in accordance with our result.

With regard to oscillator strengths (Table 7), the $^1A'(V)$ transition is the most intense one, like in CA; the oscillator strength is about 1.5 times as high as the one for the $^1A'(V')$ transition. The oscillator strength for the $^1A''(n-\pi^*)$ transition is again found to be extremely low.

Further, some analogy with respect to CA is observed with regard to the excited-state dipole moments reported in Table 4. However, both $^1A'$ excited states now exhibit an appreciable increase of their dipole moment values, as a result of the strong *V*/*V*′ mixing. The $^1A''(n-\pi^*)$ state displays a reversed dipole moment direction, similarly to the case of CA. In agreement with these observations, the charge distributions for the ground and corresponding excited states of CTA (Table 8) indicate an electron migration from the phenolic ring to the alkyl fragment in both the $^1A'(V')$ and $^1A'(V)$ states, and a reversed charge transfer in the case of $^1A''(n-\pi^*)$ state.

4. Geometry Relaxation in Excited CTA. Results of in-plane geometry optimization for the excited states of CTA are shown in Figure 3, using the EOM-CCSD data of Table 7. As in Figure 2 for CA, the stationary points corresponding to the in-plane equilibrium geometries of the respective excited states are fixed along the horizontal axis, and cuts through the S_1, S_2, and S_3 potential surfaces are shown as a function of these selected geometries. Again, the vertical excitation data corresponding to the ground state $\tilde{X}^1A'$ geometry are given as a reference.

By comparison with Figure 2 for CA, the most notable feature in the case of CTA is that the $^1A''(n-\pi^*)$ state remains the lowest excited state (S_1) at all geometries under consideration. Similarly to the observations for CA, this state is also subject to the most extensive relaxation: here, the energetic lowering is of 0.48 eV (smaller, though, than for CA). The energetic ordering of the $^1A'$ states is reversed at the $^1A''(n-\pi^*)$ geometry, which is again very likely the sign of a (conical) intersection between the $^1A'$ PESs.

The $^1A'(V')$ state was found to be subject to minor geometry relaxation effects, of about 0.04 eV. Interestingly, the $^1A'(V)$ state is predicted to lie below $^1A'(V')$ at the $^1A'(V')$ geometry. This suggests that an intersection of the PESs of these states is not far from the $^1A'(V')$ point.

Finally, the relaxation of the $^1A'(V)$ state is substantial, about 0.43 eV; however, this state still lies above the $^1A''(n-\pi^*)$ state at the $^1A'(V)$ geometry. The $^1A'(V)$ state is thus the second lowest state, with $^1A'(V')$ lying substantially higher.

The bond lengths pertaining to the excited-state stationary points for CTA are included in Table 6 and are compared there with the corresponding ground-state data. Analysis of the $^1A''(n-\pi^*)$ structure indicates that the character of the geometry alterations correlates with that observed in the case of CA. Thus, one observes a rather pronounced stretching of the $C_9=O_2$ double bond, along with a substantial contraction of the C_8-C_9 bond and a moderate elongation of the C_7-C_8 bond. As for the $^1A'(V)$ structure, it is characterized by a pronounced elongation of the C_7-C_8 bond accompanied by a moderate contraction of the C_8-C_9 bond. The resulting lengths of the C_7-C_8 and C_8-C_9 bonds are nearly identical, and almost of single bond character. In the $^1A'(V')$ state, an aromatic ring extension is again mostly involved in the relaxation.

IV. Discussion

The above observations can be summarized as follows: (i) The relevant low-lying excited singlet states of both CA and CTA are two $\pi-\pi^*$ states, $^1A'(V')$ and $^1A'(V)$, and an $n-\pi^*$ state, $^1A''(n-\pi^*)$; the underlying orbital pattern is depicted in Figure 1. (ii) The substitution oxygen → sulfur has an enormous impact on the electronic spectrum in CTA as compared with CA: the $^1A''(n-\pi^*)$ state becomes the lowest vertically excited state and, further, the lowest excited state at all in-plane geometries considered. (iii) In-plane geometry relaxation leads to a pronounced energetic re-ordering in both CA and CTA which points to the existence of several conical intersections. The prediction of the intersection between the $^1A'(V')$ and the $^1A'(V)$ excited states of CA is in agreement with recent observations by Martínez and co-workers.[8] (iv) In both CA and CTA, the $^1A''(n-\pi^*)$ state is subject to a pronounced in-plane relaxation involving elongation of the carbonyl $C_9=O_2$ double bond and contraction of the neighboring C_8-C_9 bond. In CA, the $^1A''(n-\pi^*)$ state becomes the lowest excited state at its in-plane equilibrium geometry, lower in energy than any other S_1 state (see Figure 2). (v) Significant geometry relaxation is also observed for the $^1A'(V)$ state, involving extension of the $C_7=C_8$ double bond, pointing to the role of this state in trans-cis isomerization.

In the following, interpretations are suggested for these observations.

A. The Role of Sulfur. The substitution oxygen → sulfur brings about a substantial lowering in energy of the $^1A''(n-\pi^*)$ state. This effect is most likely related to an energy increase of the nonbonding (*n*) molecular orbital when going from CA to CTA: in CTA, this MO was found to be about 1 eV higher

than in CA. By contrast, the energies of the HOMO, LUMO, and LUMO+1 molecular orbitals change to a much lesser extent. Hence, the $n \rightarrow \pi^*$ transition energy (HOMO-3 $\rightarrow$ LUMO, see Figure 1) decreases substantially.

The reason for the marked increase in energy of the nonbonding molecular orbital in CTA lies in the contribution of the $3p_x$ and $3p_y$ atomic orbitals (AOs) of sulfur to that MO. The energies of the latter AOs are much higher than the energies of the corresponding $2p_x$ and $2p_y$ AOs of the carboxyl oxygen which contribute to the nonbonding MO in the case of CA. (The ionization potentials for the 3p AO of sulfur and the 2p AO of oxygen are 10.4 and 13.6 eV, respectively.) Further, the overall weight of the sulfur AOs in the nonbonding MO of CTA is found to be about twice as high as the corresponding weight of the carboxyl oxygen in the nonbonding MO of CA. As a result, the energy of the nonbonding MO in CTA is significantly higher than in CA.

B. Geometry Relaxation of the $^1A''(n-\pi^*)$ State. The relaxation pattern of the $^1A''(n-\pi^*)$ excited state is uniform for CA and CTA. It involves a very pronounced elongation of the carbonyl C_9-O_2 double bond, halfway toward a single bond, along with a marked contraction of the C_8-C_9 single bond (Table 6). By the $n \rightarrow \pi^*$ excitation, the carbonyl π bond is apparently weakened while the adjacent carbon−carbon bond acquires double bond character. A similar pattern has recently been observed for cytosine in a study by Robb and co-workers.[39] These authors refer to an "uncoupling" of the carbonyl π bond followed by a "recoupling" with a neighboring π system. In the process, the length of the $C_7=C_8$ double bond increases by 0.04 Å (0.03 Å in CTA) as compared with the ground state. Note that this increase can be favorable for the trans−cis isomerization (see section IV.C). Although this analysis of the geometry relaxation is in agreement with the picture proposed by Robb and co-workers, one should note, though, that the interpretation given in ref 39 regarding the role of the $n-\pi^*$ state in the ultrafast photophysics of cytosine has more recently been criticized, see ref 40.

Since the $^1A''(n-\pi^*)$ state becomes the lowest excited state in CA as a result of its very extensive adiabatic relaxation, one might conjecture whether this state plays a role in the recent experimental spectroscopic observations for CA by Levy and co-workers.[17] These experiments have been interpreted so far[8,17] in terms of the two $\pi-\pi^*$ states, $^1A'(V')$ and $^1A'(V)$ in our nomenclature. Consistent with our results for the respective oscillator strengths (see section III.C.1 and Table 3), the red end of the fluorescence excitation spectrum, where transitions to the $^1A'(V')$ state are expected, is less intense, while a high-intensity region sets in toward the blue end.

Though transitions to the $^1A''(n-\pi^*)$ state have an extremely low oscillator strength (see Table 3), intensity borrowing could take place via vibronic coupling mechanisms to the $^1A'(V')$ and $^1A'(V)$ states. This can make the $^1A''(n-\pi^*)$ transitions visible in the spectrum. The presence of vibronic coupling is suggested by the broad and irregular appearance of the spectral features, especially at high energies. However, an involvement of the $^1A''(n-\pi^*)$ state would entail a characteristic vibrational structure, relating in particular to C=O stretch excitation, which cannot be discerned from the experimental (emission) spectra.[17] For a detailed interpretation of the fluorescence absorption spectrum of Levy and co-workers, calculations using the linear vibronic coupling model of ref 41 could be envisaged.

C. Perspective on trans−cis Isomerization. Photon absorption by the native PYP chromophore leads to its trans-cis isomerization with respect to the $C_7=C_8$ double bond (possibly involving a more complicated twisting process which also affects neighboring bonds).[3] The CA chromophore in the gas phase was shown to undergo the same type of photochemistry, with the yield of the reaction product showing a marked dependence on the excitation energy.[17] Although the present analysis is restricted to in-plane geometries and thus does not allow us to obtain a precise picture of the isomerization process, we comment here on certain aspects which can be inferred from our results.

By inspecting the orbital pattern of Figure 1, the trans−cis photoisomerization should very likely be initiated in the electronic state involving the HOMO−LUMO excitation pattern, i.e., a bonding $\rightarrow$ antibonding transition with respect to the C_7-C_8 bond. The electronic state which predominantly features this excitation pattern is the $^1A'(V)$ state. At the $\tilde{X}^1A'$ planar geometry, this state is the second excited state (S_2) in CA and the third excited state (S_3) in CTA. As pointed out above (section III.C), the C_7-C_8 bond significantly lengthens on geometry relaxation in this state, as expected due to the antibonding character of the dominant LUMO molecular orbital. The C_7-C_8 bond is thus stretched by 0.04 Å in CA and 0.07 Å in CTA. By comparison, geometry relaxation in the $^1A'(V')$ state does not much affect the C_7-C_8 bond. For the $^1A''(n-\pi^*)$ state, the extent of the change in bond length is comparable to the change for the $^1A'(V)$ state, 0.04 and 0.03 Å in CA and CTA, respectively, but the full occupation of the HOMO in the $^1A''(n-\pi^*)$ state suggests that the C_7-C_8 double bond character is essentially retained. Hence, isomerization is not expected to occur from the $^1A''(n-\pi^*)$ state.

Another observation from our results concerns the pronounced role of V−V′ mixing, especially in the case of CA. As pointed out in section III.C, this mixing signals an avoided crossing or conical intersection situation. This can be accompanied by a significant change in oscillator strengths: for example, in the case of CA, we have determined the oscillator strength to be 0.389 [$^1A'(V')$] vs 0.447 [$^1A'(V)$] at the $^1A'(V)$ geometry (near the $^1A'(V')/^1A'(V)$ degeneracy, see Figure 2) as compared with 0.061 [$^1A'(V')$] vs 0.739 [$^1A'(V)$] at the Franck−Condon ($\tilde{X}^1A'$) geometry. Relevant intersections could arise at the planar geometry, as can be inferred from Figures 2 and 3 (and as has been confirmed by the calculations of ref 8), and as a function of the twisting coordinate. The latter case will evidently be of key importance for the isomerization path.

These conclusions are consistent with the analysis of ref 8 relating to an S_1 barrier which occurs as a result of an S_2-S_1 avoided crossing or conical intersection in the case of CA. The presence of this barrier was previously conjectured by Levy and co-workers[17] in the context of the experimental results described in ref 17. Based upon our observations and those of refs 8 and 17, the following picture of the CA photochemistry can be suggested. We first consider the case where the S_1 state is excited. Although the S_1 state is of V′ character at the planar $\tilde{X}^1A'$ geometry (whereas S_2 is of V character), S_1 changes its electronic character V′ $\rightarrow$ V at the barrier along the "isomerization coordinate". As mentioned above and shown in ref 8, this barrier occurs as a result of the S_2-S_1 avoided crossing or conical intersection. The S_1 branch beyond the barrier is thus of V character and leads up to the S_1/S_0 intersection in the vicinity of the 90° twisted geometry.[8] For higher energies, a direct excitation of S_2 should be considered, which could involve a barrierless trans-cis isomerization along a path which would be of V character throughout. Notice, though, that the analysis of ref 8 suggests an extremely rapid decay of an initial S_2 population via an in-plane S_2-S_1 conical intersection.

According to the experimental results by Levy and coworkers,[17] the trans−cis photoisomerization in CA sets in for excitation energies higher than ∼4.27 eV (about 0.15 eV above the origin of the experimental spectrum). This energy was interpreted to be required to reach the S_1 isomerization barrier. According to ref 8, the barrier height is of 0.19 eV, consistent with the experimental prediction of 0.15 eV. A complementary estimate from our data can be obtained from the adiabatic energy of the $^1A'(V)$ state (4.84 eV), in whose vicinity the $^1A'(V)$/$^1A'(V')$ conical intersection should lie, see Figure 2, as compared with the adiabatic energy of the $^1A'(V')$ state (4.67 eV), which can be taken as the origin of the experimental spectrum. The difference of 0.17 eV is again in good agreement with the estimated barrier height from refs 8 and 17.

A conical intersection between the $^1A'(V)$ and $^1A''(n-\pi^*)$ states of CA, whose presence we conjecture in accordance with Figure 2, could be one of the reasons for the observed decrease in the isomerization yield on further increasing the excitation energy.[17] Once the $^1A'(V)$/ $^1A''(n-\pi^*)$ conical intersection becomes accessible, the system can be trapped in the $^1A''(n-\pi^*)$ state, where isomerization appears less likely. On the other hand, a trapping in the vicinity of the S_2/S_1 intersection could also be involved, as suggested in ref 8. Additional studies are required to clarify this issue.

Regarding the trans−cis photoisomerization in CTA, our above considerations regarding the HOMO−LUMO excitation pattern essentially remain relevant. Again, the $^1A'(V')$ state lies below the $^1A'(V)$ state at the $\tilde{X}^1A'$ geometry, and a conical intersection is expected to occur between the two states as can be inferred from Figure 3. Thus, V−V′ mixing is again expected to play a key role. In addition, a further mechanism should arise involving the $^1A''(n-\pi^*)$ state, which is the S_1 state in CTA at all in-plane stationary points considered here. More details on the respective roles of these, possibly competing, mechanisms will be reported in forthcoming work.

V. Concluding Remarks

The present study highlights the complexity of the electronic structure of the PYP chromophore, and its sensitive dependence on the presence of oxygen vs sulfur. In this first analysis, we have focused on a comparison of the neutral CA and CTA species. Among the main conclusions of our analysis are (i) the identification of three lowest singlet states, two close-lying π-π^* states ($^1A'(V')$ and $^1A'(V)$) and the $^1A''(n-\pi^*)$ state; (ii) the sequence of states upon vertical excitation, namely $^1A'(V')-{}^1A'(V)-{}^1A''(n-\pi^*)$ (in increasing order of energy) for CA, and $^1A''(n-\pi^*)-{}^1A'(V')-{}^1A'(V)$, for CTA; (iii) the particular role of the $^1A''(n-\pi^*)$ state, whose energetics is strongly influenced by the oxygen → sulfur substitution (see section III.C.3); this state is the lowest-lying state in CTA at all in-plane geometries considered, and becomes the lowest-lying state in CA upon extensive in-plane geometry relaxation; (iv) intrinsic geometry relaxation effects in the $^1A'(V)$ state which plays a key role in the trans-cis isomerization; (v) in-plane potential surface crossings among the $^1A'(V')$, $^1A'(V)$, and $^1A''(n-\pi^*)$ states of CA and CTA as a result of geometry relaxation effects (see Figures 2 and 3), which point to the role of conical intersections in these chromophores.

In view of the anionic nature of the PYP chromophore during the earliest stages of the photocycle, we briefly report here on prospecting calculations which we carried out for the anionic species CA^- and CTA^-. Here, a substantially different energetic ordering is observed, with the lowest excited-state being of $\pi-\pi^*$ character in both CA^- and CTA^-, the analogue of the $^1A'(V)$ state of neutral CA and CTA. Although a significant lowering of the $^1A''(n-\pi^*)$ state does occur in CTA^-, this state remains at comparatively high energies and does not change the overall energetic ordering, which remains the same for CTA^- as compared with CA^-. However, effects of geometry relaxation, in addition to the stabilization by the protein environment, may play a role in lowering the energy of this state. This is beyond the scope of the present work.

The electronic structure properties of the anionic vs neutral species should be considered as "limiting cases". The stabilization of the excited states via the redistribution of the negative charge between the chromophore and neighboring amino acid residues or solvent molecules play an important role in native PYP.[10,21] It will therefore be essential to include the environment explicitly at the electronic structure level. Clearly, the combined, correlated effects of oxygen/sulfur substitution, the anionic/neutral nature of the chromophore, and the properties of the chromophore's local environment determine the specific excited-state properties of the PYP chromophore.

Acknowledgment. Financial support by a DFG/CNRS collaboration project is gratefully acknowledged. We thank Casey Hynes, Alexandre Trofimov, Todd Martínez, Monique Martin, Pascale Changenet-Barret, and Riccardo Spezia for valuable discussions. We thank our referees for helpful remarks.

Supporting Information Available: CCSD Cartesian coordinates of geometries discussed in the text are available. This material is available free of charge via the Internet at http://pubs.acs.org.

References and Notes

(1) Sprenger, W. W.; Hoff, W. D.; Armitage, J. P.; Hellingwerf, K. J. *J. Bacteriol.* **1993**, *175*, 3096.

(2) Hellingwerf, K. J.; Hendriks, J.; Gensch, T. *J. Phys. Chem. A* **2003**, *107*, 1082.

(3) Genick, U. K.; Soltis, S. M.; Kuhn, P.; Canestrelli, I. L.; Getzoff, E. D. *Nature* **1998**, *392*, 206.

(4) Baca, M.; Borgstahl, G. E. O.; Boissinot, M.; Burke, P. M.; Williams, D. R.; Slater, K. A.; Getzoff, E. D. *Biochemistry* **1994**, *33*, 14369.

(5) Borgstahl, G. E. O.; Williams, D. R.; Getzoff, E. D. *Biochemistry* **1995**, *34*, 6278.

(6) Genick, U. K.; Borgstahl, G. E. O.; Kingman, N.; Ren, Z.; Pradervand, C.; Burke, P. M.; Šrajer, V.; Teng, T.-Y.; Schildkamp, W.; McRee, D. E.; Moffat, K.; Getzoff, E. D. *Science* **1997**, *275*, 1471.

(7) Getzoff, E. D.; Gutwin, K. N.; Genick, U. K. *Nat. Struct. Biol.* **2003**, *10*, 663.

(8) Ko, C.; Levine, B.; Toniolo, A.; Manohar, L.; Olsen, S.; Werner, H.-J.; Martínez, T. J. *J. Am. Chem. Soc.* **2003**, *125*, 12710.

(9) Toniolo, A.; Granucci, G.; Martínez, T. J. *J. Phys. Chem. A* **2003**, *107*, 3822.

(10) Groenhof, G.; Bouxin-Cademartory, M.; Hess, B.; de Visser, S. P.; Berendsen, H. J. C.; Olivucci, M.; Mark, A. E.; Robb, M. A. *J. Am. Chem. Soc.* **2004**, *126*, 4228.

(11) Mataga, N.; Chosrowjan, H.; Taniguchi, S.; Hamada, N.; Tokunaga, F.; Imamoto, Y.; Kataoka, M. *Phys. Chem. Chem. Phys.* **2003**, *5*, 2454.

(12) Changenet-Barret, P.; Espagne, A.; Charier, S.; Baudin, J.-B.; Jullien, L.; Plaza, P.; Hellingwerf, K. J.; Martin, M. M. *Photochem. Photobiol. Sci.* **2004**, *8*, 823.

(13) Changenet-Barret, P.; Plaza, P.; Martin, M. M. *Chem. Phys. Lett.* **2001**, *336*, 439.

(14) Changenet-Barret, P.; Espagne, A.; Katsonis, N.; Charier, S.; Baudin, J.-B.; Jullien, L.; Plaza, P.; Martin, M. M. *Chem. Phys. Lett.* **2002**, *365*, 285.

(15) Larsen, D. L.; Vengris, M.; van Stokkum, I. H. M.; van der Horst, M. A.; Cordfunke, R. A.; Hellingwerf, K. J.; van Grondelle, R. *Chem. Phys. Lett.* **2003**, *369*, 563.

(16) Larsen, D. S.; Vengris, M.; van Stokkum, I. H. M.; van der Horst, M. A.; de Weerd, F. L.; Hellingwerf, K. J.; van Grondelle, R. *J. Biophys.* **2004**, *86*, 2538.

(17) Ryan, W. L.; Gordon, D. J.; Levy, D. H. *J. Am. Chem. Soc.* **2002**, *124*, 6194.
(18) Espagne, A.; Changenet-Barret, P.; Charier, S.; Baudin, J.-B.; Jullien, L.; Plaza, P.; Martin, M. M. In *Femtochemistry and Femtobiology*; Martin, M. M., Hynes, J. T., Eds.; Elsevier: Amsterdam, 2004; p 417.
(19) Molina, V.; Merchán, M. *Proc. Natl. Acad. Sci.* **2001**, *98*, 4299.
(20) Thompson, M. J.; Bashford, D.; Noodleman, L.; Getzoff, E. D. *J. Am. Chem. Soc.* **2003**, *125*, 8186.
(21) Groenhof, G.; Lensink, M. F.; Berendsen, H. J. C.; Snijders, J. G.; Mark, A. E. *Proteins* **2002**, *48*, 202.
(22) Yamada, A.; Ishikura, T.; Yamato, T. *Proteins* **2004**, *55*, 1070.
(23) He, Z.; Martin, C. H.; Birge, R.; Freed, K. *J. Phys. Chem. A* **2000**, *104*, 2939.
(24) According to our EOM-IP/6-31G* calculations the first ionozation potential of the deprotonated CTA is 2.88 eV whereas its first excited-state lies at 3.04 eV.
(25) Sekino, H.; Bartlett, R. J. *Int. J. Quantum Chem., Quantum Chem. Symp.* **1984**, *18*, 255.
(26) Geertsen, J.; Rittby, M.; Bartlett, R. J. *Chem. Phys. Lett.* **1989**, *164*, 57.
(27) Stanton, J. F.; Bartlett, R. J. *J. Chem. Phys.* **1993**, *98*, 7029.
(28) Stanton, J. F. *J. Chem. Phys.* **1993**, *99*, 8840.
(29) http://www.vitamins-minerals.tv/phytochemicals/para_coumaric_acid.htm.
(30) Purvis, G. D.; Bartlett, R. J. *J. Chem. Phys.* **1982**, *76*, 1910.
(31) Dunning, T. H. *J. Chem. Phys.* **1989**, *90*, 1007.
(32) The minimum type of the ground-state equilibrium structure was verified by additional geometry optimization calculations where a less-symmetrical initial configuration of the molecule was used. No other stationary points were obtained in those cases.
(33) ACES II is a program product of the quantum theory project. Stanton, J.; Gauss, J.; Watts, J.; Nooijen, M.; Oliphant, N.; Perera, S. A.; Szalay, P. G.; Lauderdale, W. J.; Kucharski, S. A.; Gwaltney, S. R.; Beck, S.; Balková, A.; Bernholdt, D. E.; Baeck, K. K.; Rozyczko, P.; Sekino, H.; Hober, C.; Bartlett, R. J.
(34) Molpro, version 2002.1, a package of ab initio programs. Werner, H.-J.; Knowles, P. J.; Lindh, R.; Schütz, M.; Celani, P.; Korona, T.; Manby, F. R.; Rauhut, G.; Amos, R. D.; Bernhardsson, A.; Berning, A.; Cooper, D. L.; Deegan, M. J. O.; Dobbyn, A. J.; Eckert, F.; Hampel, C.; Hetzer, G.; Lloyd, A. W.; McNicholas, S. J.; Meyer, W.; Mura, M. E.; Nicklass, A.; Palmieri, P.; Pitzer, R.; Schumann, U.; Stoll, H.; Stone, A. J.; Tarroni, R.; Thorsteinsson, T. **2002**.
(35) Foresman, J. B.; Head-Gordon, M.; Pople, J. A.; Frisch, M. J. *J. Phys. Chem.* **1992**, *96*, 135.
(36) Sergi, A.; Grüning, M.; Ferrario, M.; Buda, F. *J. Phys. Chem. B* **2001**, *105*, 4386.
(37) Truhlar, D. G.; Mead, C. A. *Phys. Rev. A* **2004**, *68*, 032501.
(38) Olivucci, M.; Robb, M. A.; Bernardi, F. In *Conformational Analysis of Molecules in Excited States*; Waluk, J., Ed.; Wiley-VCH: New York, 2000; pp 297−366.
(39) Ismail, N.; Blancafort, L.; Olivucci, M.; Kohler, B.; Robb, M. A. *J. Am. Chem. Soc.* **2002**, *124*, 6818.
(40) Merchán, M.; Serrano-Andrés, L. *J. Am. Chem. Soc.* **2003**, *125*, 8108.
(41) Köppel, H.; Domcke, W.; Cederbaum, L. S. *Adv. Chem. Phys.* **1984**, *57*, 59.